ORIGINAL PAPER

Analysis and optimisation of titanium alloy sandwich structures for thermal protection

Philipp Nieke[1] · Valerie Chopovda[1] · Nicholas J. Rattenbury[2] · John E. Cater[3]

Abstract

The heat transfer through additively manufactured Ti–6Al–4V sandwich structures has been investigated by simulating a one-dimensional multi-layer transient problem for heat fluxes up to $100 \ \mathrm{kW \ m^{-2}}$. A previously published model for graded titanium foam insulation has been adapted, and its performance was validated experimentally for the additively manufactured titanium alloy samples. The optimal solidity distribution to minimise the peak temperature for a transient heat flux has been produced for a given sample mass and total thickness. The optimal distribution consists of three layers: the two outer layers are solid, the middle layer has the lowest possible solidity, and most of the material is distributed furthest from the applied heat flux.

Keywords Sandwich structure · Lattice · Metallic thermal protection systems · Electron beam melting · Ti–6Al–4V

1 Introduction

Among the conventional metals used in additive manufacturing, the titanium alloy Ti–6Al–4V has the highest melting interval (> 1600 °C) and the lowest thermal conductivity—two beneficial properties for the design of a metal thermal protection system (TPS). Additionally, Ti–6Al–4V is an established aerospace material [7] and showed high resistance to demise when exposed to high-heat flux conditions in ground testing facilities [14]. However, a drawback of metal TPSs is their relatively high mass. To minimise mass, metal TPSs are commonly based on sandwich structures with porous cores and solid face sheets that exhibit a high stiffness-to-weight ratio [1].

Various sandwich core configurations, such as metal foams [5, 18], corrugated cores [3, 8, 9] or honeycombs [10] were discussed in the literature. However, more recently additively manufactured cores have been presented as providing greater design flexibility [12, 16]. Lin et al. [12] studied an integrated TPS with a core based on the biological structure of the Norway spruce. The authors simulated and tested four designs to temperatures up to 300 °C. All samples were produced in Ti–6Al–4V by selective laser melting. In another study by Xu et al. [16], additively manufactured lattice core sandwich structures made of Ti–6Al–4V and/or C/SiC were simulated and tested using a blow torch.

This paper investigates the performance of Ti–6Al–4V sandwich structures with lattice cores for heat fluxes of up to $100 \ \mathrm{kW \ m^{-2}}$. The transient thermal behaviour is predicted using a one-dimensional numerical model based on previous work on the performance of titanium foam insulation [18]. An adapted model is validated using an experimental set-up with a custom-built heat gun apparatus. An optimisation strategy is then applied to achieve an optimal solidity profile throughout the sample to minimise heat transfer to the support structure.

✉ Philipp Nieke
p.nieke@auckland.ac.nz

Valerie Chopovda
valerie.chopovda@auckland.ac.nz

Nicholas J. Rattenbury
n.rattenbury@auckland.ac.nz

John E. Cater
john.cater@canterbury.ac.nz

1 Department of Engineering Science, The University of Auckland, Auckland, New Zealand

2 Department of Physics, The University of Auckland, Auckland, New Zealand

3 Department of Mechanical Engineering, University of Canterbury, Christchurch, New Zealand

2 Model formulation

2.1 Previous model

The model considered in Zhu et al.[18] consists of a (pure) titanium foam insulation panel and an aluminium structural mass attached to the panel from the cool side. The insulation panel comprises two layers, and the solidity is uniform within each layer. The total insulation thickness is $h = 0.2$ m.

The one-dimensional transient heat conduction problem is specified by

$$\frac{\partial}{\partial x}\left(k\frac{\partial T}{\partial x}\right) = \rho_f \, C_p \frac{\partial T}{\partial t},$$

with $T(0) = T_{amb}$, where ρ_f is the titanium foam density, and C_p is the constant specific heat capacity of titanium at $T_{amb} = 26.85\,°C$ (300 K).

Figure 1 shows the associated model geometry.

On the front face, a transient one-dimensional heat flux of $q_i = 56,745$ W m^{-2} is applied for $t_0 = 2,000$ s and then removed. The front face of the insulation panel radiates heat to the environment. The front face's emissivity is constant and assumed to be unity [17].

The back face boundary conditions assume that there is conduction between the insulation panel and the aluminium structural mass that constitutes the wall of a pressure vessel. The structural mass is insulated from the inside.

Zhu et al. [18] found an optimal design for a two-layer structure of the insulation panel so that the maximum cool-side temperature max(T_{back}) is minimal. The design of the insulation panel is constrained by the constant total thickness h and fixed areal mass density $m_p = 22.15$ kg m^{-2} of the panel.

The titanium foam insulation is modelled using an idealised uniform cubic cell structure with fixed strut diameter $d_s = 0.05$ mm. Only low-density foams were considered in the study; the solidity s of the layers varies between $s_{min} = 0.01$ and $s_{max} = 0.11$. Variation in solidity

is achieved by changing the cell size b, which, therefore, determines the volume fraction of metal in the open-cell foam,

$$s = \frac{3}{4}\pi\left(\frac{d_s}{b}\right)^2. \tag{1}$$

The thermal conductivity for open-cell titanium foam is calculated by linearly combining the three main heat transfer modes in this application: air conduction, metal conduction and radiation. The effective thermal conductivity is:

$$k_{eff} = (1 - s)k_{air} + \frac{1}{3}k_{metal}\, s + k_{rad}, \tag{2}$$

with expressions for k_{air}, k_{metal} and k_{rad} [15]. The open-cell expression for k_{rad} (Equation 10 in [15]) is a function of the emissivity of the material. In the present work, the titanium emissivity inside the foam was set to $\varepsilon = 0.5$ [15], while the front face emissivity has a value of 1.0, consistent with the assumptions of the previous model.

The optimisation problem is formulated as:

$$\min_{h_1, s_1}\left\{\max_t\left[T_{back}(h_1, s_1, t)\right]\right\},$$

with the following bounds and constraints on the design variables h_1, h_2, s_1, s_2:

$$h_1 s_1 + h_2 s_2 = \frac{m_p}{\rho_{metal}}, \tag{3}$$

$$h_1 + h_2 = h, \tag{4}$$

$$0.01 \le h_1 \le 0.19 \text{ m},$$
$$0.01 \le h_2 \le 0.19 \text{ m},$$
$$0.01 \le s_1 \le 0.11, \tag{5}$$
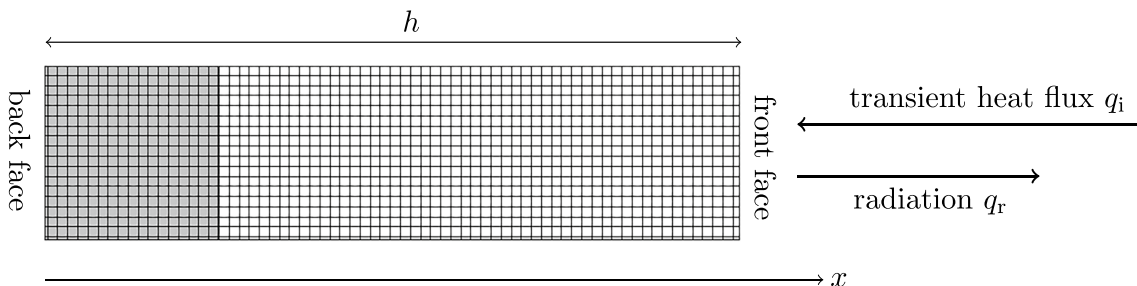
$$0.01 \le s_2 \le 0.11. \tag{6}$$

Fig. 1 Schematic of the geometry of the titanium foam insulation used by Zhu et al.[18]. An optimiser was used to determine the thickness and solidity of each of the two layers

Table 1 Comparison between [18, Table 1], and the Current Model

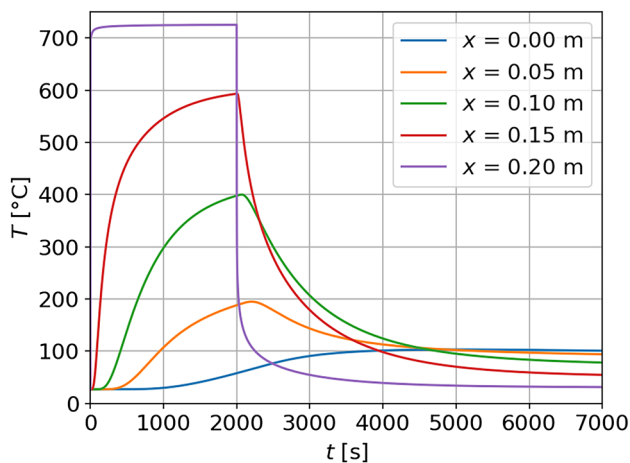| Solidity Distribution	Optimal		Extreme		Uniform	
Model	Zhu et al	Current	Zhu et al	Current	Zhu et al	Current
Cool-side h_1 [m]	0.0162	0.0300	0.0300		N/A	
Cool-side solidity s_1	0.1100		0.1100		0.025	
Hot-side h_2 [m]	0.1838	0.1700	0.1700		N/A	
Hot-side solidity s_2	0.0175	0.0100	0.0100		0.025	
$\max(T_{\text{back}})$ [°C]	198.0	103.1	225.7	103.1	215.5	160.4
$t(\max(T_{\text{back}}))$ [s]	4,203.7	5,041.5	3,115.0	5,041.5	4,572.0	5,571.8

Fig. 2 The temperatures at different locations within the current optimal two-layer design using k_{rad} for open-cell foam in Table 1
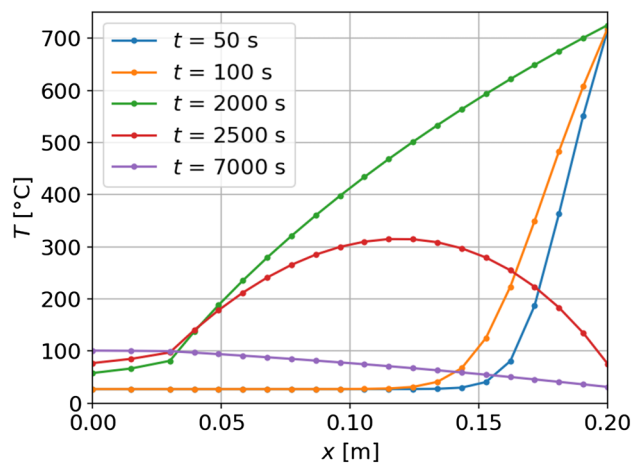

Fig. 3 The temperature profiles in the current optimal two-layer design in Table 1 at different instants in time

The optimisation search was initialised with values of $s_1 = s_2 = 0.025$, and $h_1 = h_2 = h/2$.

Zhu et al. [18] solved this problem using MATLAB's *fmincon* function for constrained nonlinear optimisation, with the sequential quadratic programming (SQP) algorithm. In the present work, the sequential least squares programming (SLSQP) method for constrained nonlinear optimisation was used from Python's *scipy.optimize.minimize* package with similar parameters.

Table 1 compares the results of the current model with the previously published results. Note that the previous results differ slightly which can be explained by a discrepancy in the definition of the thermal conductivity model (i.e. Equation A.5 in [15]) was used rather than Equation 10 in [15]).

Figures 2 and 3 show the temperatures at different locations and instants within the model insulation panel for the optimised design. In the current model, it takes more time for the cool side to reach the maximum temperature, so the integration time was increased from 5000 s to 7000 s.

The optimal design in the current model is the same as the extreme design, with the maximum back-side temperature of 103.1 °C (376.2 K) at 5,041.5 s. The current model gives a higher maximum front temperature $\max(T_{\text{front}})$ of 125.7 °C

(398.8 K) at 5,715 s, which is more than 20 °C higher than the optimal design presented by Zhu et al. [18].

2.2 Adapted model for higher-density cellular solids

In the previous work of Zhu et al. [18], only low-density foams were considered. Relaxing the maximum value constraint makes it possible to achieve purely solid layers with solidity $s = 1$; the solidity constraints (5), (6) then become,

$$0.01 \leq s_1 \leq 1.00,$$
$$0.01 \leq s_2 \leq 1.00.$$

Note that when $s = 1$, both k_{rad} and k_{air} become zero, as there are no internal voids, and thus no radiation. Also, the term for metal conduction in its original form in Equation (2) is not valid for $s = 1$. This problem was resolved by replacing it with the expression for thermal conductivity of a porous solid suggested by Ashby[1]:

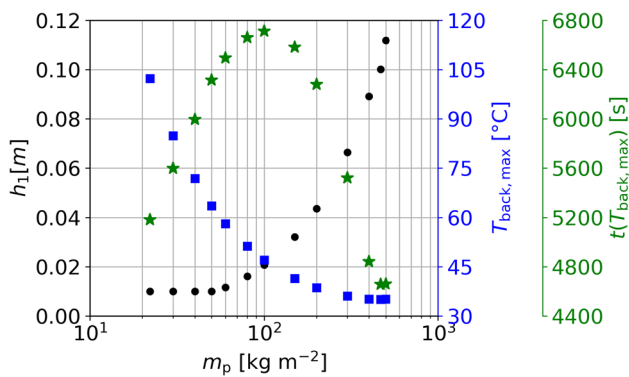$$\frac{1}{3} k_{\text{metal}} \left(s + 2s^{3/2} \right).$$

Fig. 4 Optimisation results of the revised model for different areal densities m_p. Black circles represent the thickness of the back layer h_1, blue squares depict the maximum temperature at the back layer $T_{back,\,max}$ and the green stars show at what time the maximum temperature at the back layer $t(T_{back,\,max})$ is reached

2.3 Areal mass density

Another constraint in the initial model was the fixed areal mass density m_p of the insulation panel. This constraint was successfully relaxed and removed to investigate the effect of an increasing areal density. Figure 4 summarises the optimisation results of the revised model with relaxed solidity constraints for different areal mass densities m_p.

The first point on the left represents the state of the system with the same areal mass density of $m_p = 22.15$ kg m^{-2} as in the previous optimisation. Permitting higher solidities results in a thinner and denser back layer (cold side), while the front layer (hot side) becomes thicker and less solid. This reduces the maximum temperature on the back face by less than 1 °C, but it takes approximately 140 s longer to reach the maximum value.

The first four optimisations show that the back layer thickness h_1 remains constant. As the allowed mass of the insulation panel is increased, the back layer's solidity rises until it becomes 1.0. Once this is achieved (m_p between 50 kg m^{-2} and 60 kg m^{-2}), the thickness of the cool-side layer starts to increase as well. The maximum temperature at the back decreases, and the time to reach it increases as the heat capacity of the back layer is increased. In contrast, the hot-side layer is as thick and as porous as possible, with the minimum permitted solidity. Its thickness decreases only to maintain the sample's total thickness.

At an areal mass density of approximately 100 kg m^{-2}, the time to reach the maximum temperature peaks at approximately 6713 s. Adding more mass to the panel does not delay the occurrence of the maximum temperature further, as higher solidity results in a higher effective thermal conductivity, thus facilitating heat transfer to the back.

The profile for $m_p = 465.83$ kg m^{-2} corresponds to the model with unfixed areal mass density. For this design, the optimisation model suggests that the layers are almost equal in thickness (the back layer is only slightly thicker). The maximum back sheet temperature is at its minimum of approximately 35 °C.

Overall, the results of the optimisation model suggest that it is preferable to have most material at the back of the insulation panel. A thin but dense back layer is more efficient than a thicker and less dense layer. The balance between effective thermal conductivity and heat capacity results in an optimum time to reach the maximum back face temperature.

3 Experimental validation

3.1 Lattice core samples

To investigate the thermal protection properties of lattices that could be functionally graded, cylindrical titanium alloy (Ti–6Al–4V) sandwich samples were designed using engineering design software (nTopology Inc.). They were printed by a commercial additive manufacturing service on Arcam machines (GE Additive) using Electron Beam Melting. An example of a manufactured sample is shown in Fig. 5.

The front and the back face sheets are completely solid except for the three mounting holes at the back. The sandwich core consists of a volume lattice and a surface lattice (to cover the curved lateral surface). Both lattices are based on a body-centred cubic unit cell with an edge length of 5 mm. To ensure a gradual change of cross-sections between the core lattice and the solid face sheets, fillets with a radius of 2 mm are added. Two sample thicknesses and two strut diameters were realised. The smallest realised strut diameter
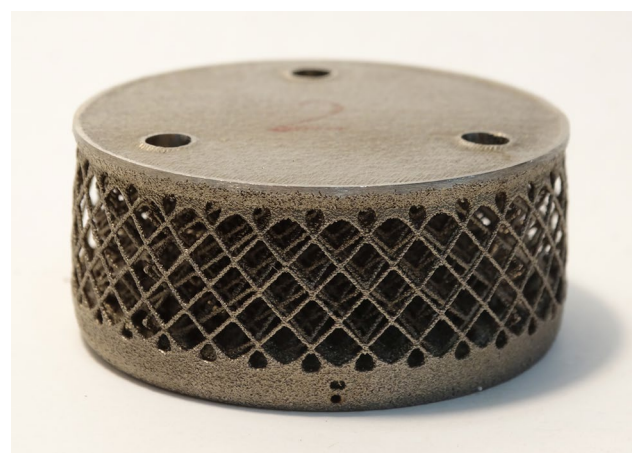

Fig. 5 An example of a printed Ti–6Al–4V sandwich sample with a diameter of 50 mm. The front face is pointing down and is separated from the back face by a regular lattice based on a body-centred cubic unit cell. The back face is on top and is shown with 3 holes that are used for mounting the sample

was 0.5 mm, to ensure structural integrity. Table 2 summarises the sample parameters.

3.2 Testing apparatus

The experimental validation was performed in a custom-built testing apparatus that consists of a sample holder and a heat gun (Bosch, GHG 20-63). Figure 6 shows a schematic diagram and a photo of a sample mounted in the testing apparatus. The back and sides of the lattice core sample were insulated using ceramic fibre board. The sample's front face was exposed to a hot air jet.

Temperatures were measured using four mineral insulated type K thermocouples (RS Pro) with a diameter of 0.5 mm and a datalogger (Pico Technology, TC-08). One thermocouple was positioned in a hole in the solid front sheet, and

a second thermocouple in a hole in the back sheet. The thermocouple holes are parallel to the faces and have a depth of approximately 23 mm to measure temperatures close to the centre line of the sample.

All tests were conducted at an ambient temperature of $T_{amb} \approx 24\,°C$. The heat gun was set to a moderate temperature $T_{hg} = 300\,°C$ to exclude any material alterations such as oxidation during the tests. The heat gun was positioned such that the distance between the front surface of the sample and the nozzle outlet was 40 mm. At the beginning of each test, the sample was protected by a ceramic fibre board cover to prevent heating while the heat gun reached the set operating temperature (≥ 10 s). The cover was removed by pulling a mounting pin, and simultaneously, the collection of temperature measurements commenced. The test duration for each sample was 600 s.

3.3 Modelling of lattice core samples

The adapted model of Sect. 2.2 was used for the numerical simulation of the samples. A five-layer design is utilised, as shown in Fig. 7. The first and the fifth layers are solid metal sheets with solidity very close to one $s_1 = s_5 = 0.99$ (The solidity of 0.99 was assumed to account for any potential residual porosity from the additive manufacturing process).

The second and the fourth layers are thin (2 mm) transitional layers between solid sheets and the lattice core (third layer) in-between. The parameters used for modelling the samples are the same as those presented in Table 2.

As with the previous model, for each layer, the cubic cell size b is fixed with variable strut diameter d_s, and related to the solidity s by Equation (1). As the present samples were made of the Titanium alloy Ti–6Al–4V (rather than pure Titanium), temperature-dependent relations from published sources were implemented for density [13], specific heat capacity [4] and emissivity [2].

The thermal conductivity model only includes terms for air and metal conduction. The radiation term k_{rad} was

Table 2 Parameters of lattice core samples

Parameter	Unit	Sample 1	Sample 2	Sample 3	Sample 4
Total thickness* h	mm	21.65	21.02	31.76	31.18
Strut diameter+ d_s	mm	0.5	1.0	0.5	1.0
Thickness* h_1	mm	2.5	2.71	2.28	2.91
Thickness+ h_2, h_4	mm	2	2	2	2
Thickness# h_3	mm	10.77	9.75	20.99	19.76
Thickness* h_5	mm	4.38	4.55	4.485	4.51
Solidity& s_1, s_5	1	0.99	0.99	0.99	0.99
Solidity+ s_2, s_4	1	0.2054	0.3265	0.2354	0.3365
Solidity* s_3	1	0.0402	0.1114	0.0402	0.1314
Mass* m	g	67.04	81.17	71.16	94.88
Diameter+ d	mm	50	50	50	50
Mass Density# m_p	kg m^{-2}	34.14	41.34	36.24	47.87

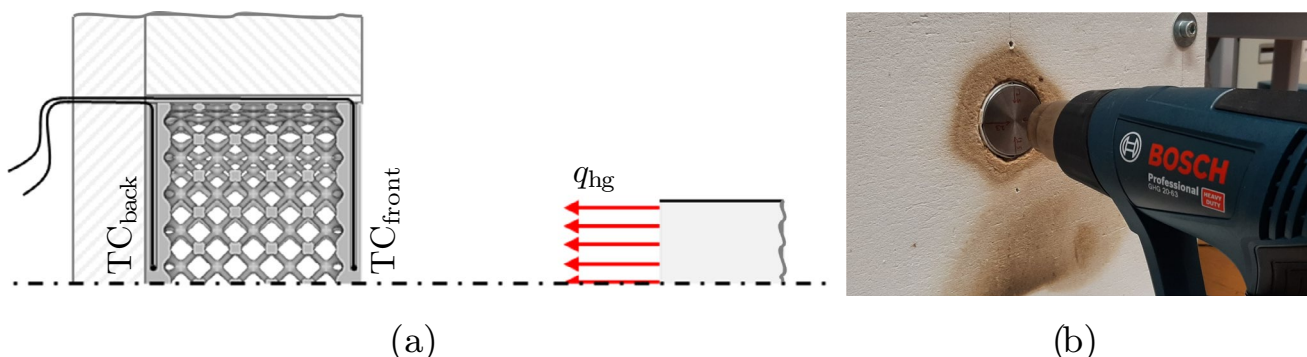* Measured, + Nominal, # Calculated, & Assumed

(a)   (b)

Fig. 6 **a** Schematic diagram and **b** lattice core sample mounted in the heat gun apparatus. The positions of thermocouples within the front and the back face sheets of the sample are denoted respectively

Fig. 7 The schematic of the initial model geometry shows layers with different solidities and, hence, thermal properties. Layers 1 and 5 represent solid face sheets, layer 3 is a low-solidity lattice core, and layers 2 and 4 are transitional layers of intermediate solidity
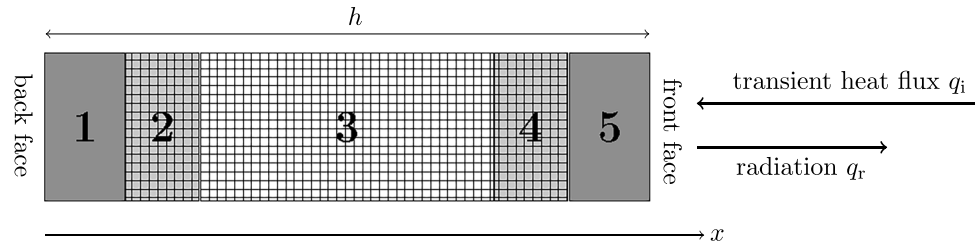
omitted since radiation is negligible for the relatively small temperature differences evident at these low temperatures, and it is assumed that the other surfaces have adiabatic boundary conditions. The metal conduction model uses the revised term suggested by Ashby [1], so that the total effective thermal conductivity is given by

$$k_{\text{eff}} = (1 - s)k_{\text{air}} + \frac{1}{3}k_{\text{metal}}\left(s + 2s^{3/2}\right), \tag{7}$$

with k_{metal} for Ti–6Al–4V derived from Boivineau et al. [6].

The model boundary conditions are selected to match the experimental conditions: an insulated back face ($x = 0$), and forced convection and radiation on the front face ($x = h$):

$$q(0, t) = 0,$$
$$q(h, t) = A\, h_{\text{hg}}(T_{\text{hg}} - T(h, t)) - A\varepsilon\sigma(T^4(h, t) - T_{\text{amb}}^4),$$

where A is the cross-sectional area, which is unity for a one-dimensional problem, ε is the front surface emissivity of the sample, and σ is the Stefan–Boltzmann constant. The assumed convective heat transfer coefficient $h_{\text{hg}} = 120\,\text{W}\,\text{m}^{-2}\,\text{K}^{-1}$ is within a typical range of coefficients for the forced convection in gases given by Incropera et al. [11].

3.4 Validation results

The experimentally derived temperatures are shown in Fig. 8 in comparison with the numerical results. The final front face temperature in the model solutions is always higher than measured in the experiment, which is expected since it is likely that there are additional losses in the experiment. The value of the convective heat transfer coefficient h_{hg} also has a relatively large associated uncertainty as it was not measured.

Table 3 provides a summary of the maximum temperatures at 600 s and the root-mean-square error (RMSE).

The absolute differences in the back face temperatures vary between 2 °C and 20 °C. Given the cubic lattice approximation and the assumption of uniform material properties within each layer, these discrepancies are considered to be acceptable for this one-dimensional model. The actual lattice solidity is also difficult to estimate, particularly for the transitional layers. Overall, the performance of the numerical

model in predicting the back face temperature at the end of the simulation is satisfactory with the RMSE within 10 °C, which is less than 3 % in the worst case.

4 Optimisation for higher peak heat fluxes

4.1 Optimisation problem

The validated model was incorporated into the optimisation process as outlined by Zhu et al. [18] to determine the optimal solidity distribution of the samples for an increased peak heat flux.

Constraints were imposed on the number of layers, their thickness and solidity. The total thickness was fixed for each sample, and two values were considered: $h = 20$ mm and $h = 30$ mm. The solid layers at the front and back of the sample were always considered part of the structure. Their thickness was reduced to $h_f = 2$ mm to lower the final sample mass. It was assumed that there is no transition layer, and the change in solidity between layers happens immediately.

The smallest considered strut diameter was 0.5 mm (this is a common manufacturing constraint). Equation (1), between solidity s, strut diameter d_s, and open cubic cell size b, establishes the lower bound on the solidity of each layer. The smaller the cell size, the higher the minimum possible solidity. For example, when $b = 2$ mm, $s_{\text{min}} = 14.7$ %. For $b = 3.5$ mm, $s_{\text{min}} = 4.8$ %. For inner layers, the minimum cell size b was selected to be no less than $b_{\text{min}} = 2.6$ mm, so that $s_{\text{min}} = 8.71$ %.

Initially, the number of inner layers was specified as $n = 5$. Therefore, the smallest possible layer has $h_{\text{min}} = b_{\text{min}} = 2.6$ mm because a layer cannot be smaller than a cell within the layer.

The total mass of the sample was fixed as Sect. 2.3 showed that the optimised result may become too massive for an intended implementation if mass is not restricted. The masses of Samples 2 and Sample 4 from Table 2 were used for samples that are 20 mm and 30 mm thick, respectively. A variation of the mass constraint shown in Equation (3) in the form of Equation (9) was implemented in the model.
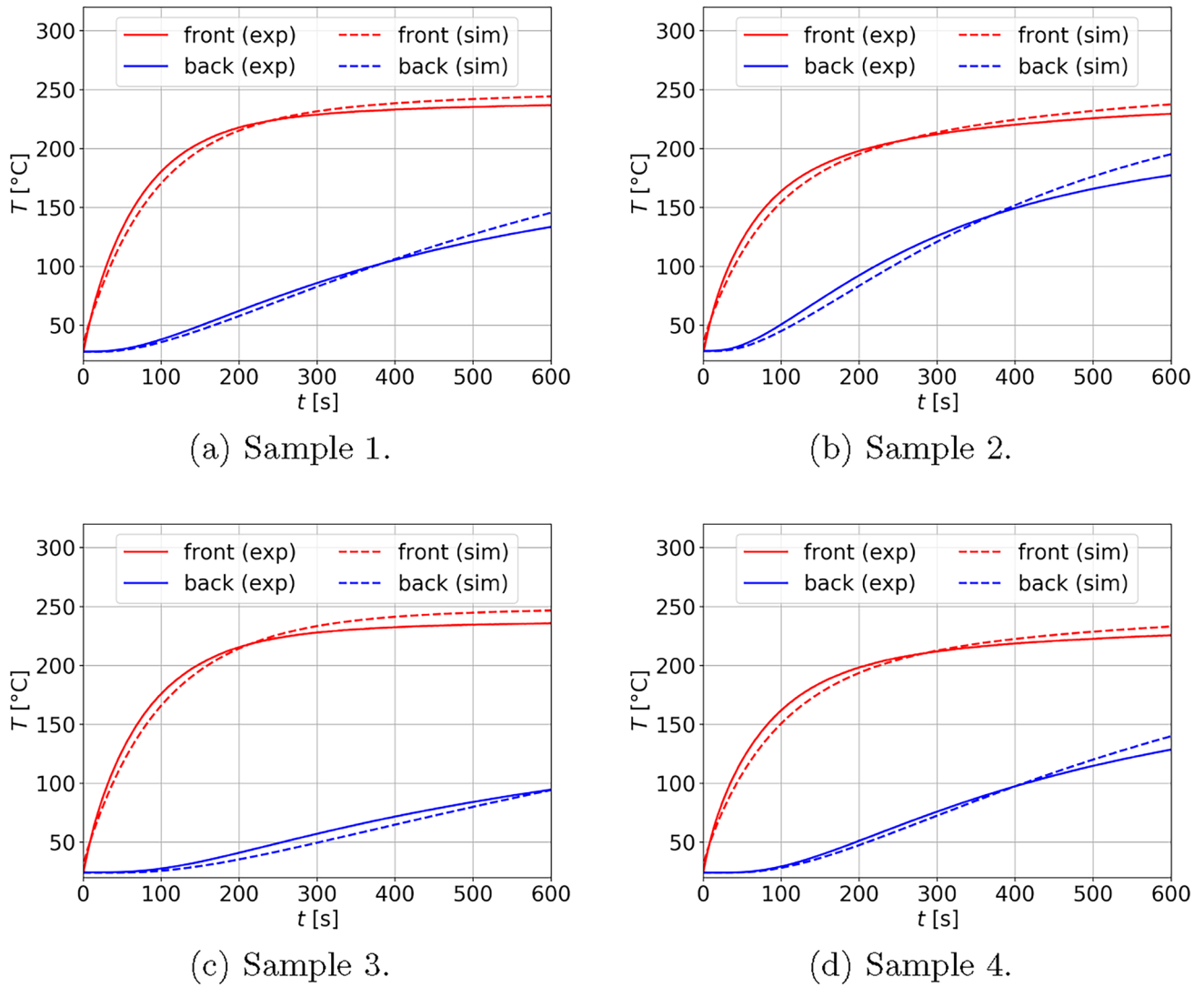
The optimisation problem is formulated as

(a) Sample 1.

(b) Sample 2.

(c) Sample 3.

(d) Sample 4.

Fig. 8 Experimental data for sample front and back sheet temperatures compared to numerical model predictions. The solid lines show the average temperatures as measured within the front and back sheets of the samples. The numerical simulation results are shown using dashed lines

Table 3 Maximum temperatures at $t = 600$ s

		Experiment [°C]	Model [°C]	RMSE [°C]
Sample 1	$\max(T_{\text{front}})$	236.7	244.2	6.3
	$\max(T_{\text{back}})$	133.4	145.5	4.7
Sample 2	$\max(T_{\text{front}})$	229.4	237.5	5.9
	$\max(T_{\text{back}})$	177.3	195.2	8.0
Sample 3	$\max(T_{\text{front}})$	235.8	246.6	8.2
	$\max(T_{\text{back}})$	94.5	94.2	5.1
Sample 4	$\max(T_{\text{front}})$	225.5	233.0	6.5
	$\max(T_{\text{back}})$	128.5	139.9	4.2

$$\min_{h_i, s_i} \left\{ \max_t \left[T_{\text{back}}(h_i, s_i, t) \right] \right\}, \tag{8}$$

such that:

$$\sum_{i=1}^{n} h_i s_i = \frac{m}{\rho_{\text{metal}} A}, \tag{9}$$

$$\sum_{i=1}^{n} h_i = h - 2h_f, \tag{10}$$

$$h_{\min} \leq h_i \leq h - 2h_f - 4h_{\min} \quad \text{for } i = 1, \ldots, n, \tag{11}$$

$$s_{\min} \leq s_i \leq 1.00 \quad \text{for } i = 1, \ldots, n, \tag{12}$$

where m is the sample mass, A is the cross-sectional area of the sample ($A = 0.00194$ m^2), and the density of Ti–6Al–4V at $T_{\text{amb}} = 23\,°C$ is $\rho_{\text{metal}} = 4420$ kg m^{-3} [13].

For the TPS optimisation, the model's boundary conditions were updated so that more extreme conditions are reached. For each model, a heat flux of $q_i = 100$ kW m^{-2} was applied for $t_0 = 180$ s, and energy radiating from the front surface to the environment is included. This corresponds to a radiation equilibrium temperature of approximately $990\,°C$, assuming an emissivity of $\varepsilon = 0.7$ at this temperature. As before, the sample is insulated at the back ($x = 0$) and from the sides. The model is solved for a simulation time interval of 600 s, and the boundary conditions are as follows:

$$q(0, t) = 0,$$

$$q(h, t) = \begin{cases} q_i - \varepsilon\sigma(T^4(h,t) - T^4_{\text{amb}}) & t \leq t_0, \\ -\varepsilon\sigma(T^4(h,t) - T^4_{\text{amb}}) & t > t_0. \end{cases} \quad (13)$$

Another 'simplified' optimisation strategy was tested, with solidity s as the only optimisation variable, a constraint that all inner layers in the sample have equal thickness, and h_i is defined at the beginning of the optimisation loop. In this model, the constraints (9) and (12) remain, but constraints (10) and (11) were not used. In summary, two cases were investigated; inner layers with variable thickness and inner layers with equal thickness.

4.2 Optimisation results

The results for the first case are shown in Fig. 9. The optimiser was initialised with a sample structure of two outer solid sheets and $n = 5$ equal inner layers with $h_i = (h - 2h_f)/n$ and $s_i = 0.25$, $i = 1, \ldots, n$. Note that the optimiser attempts to transfer mass to the back of the sample to reduce the maximum temperature achieved. This is
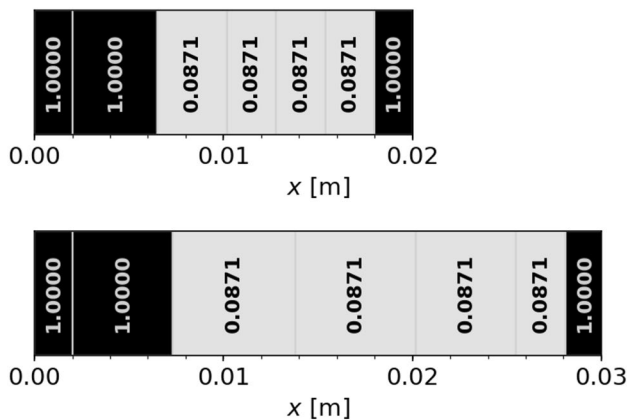
Fig. 9 Solidity profiles for the two optimised samples with five inner layers of variable thickness. The solidity values are shown inside each layer—the denser the layer, the darker the grey

consistent with the results of the previous work [18] presented in Sect. 2. In all cases, the optimised solution essentially consists of three layers: two thin solid layers and one thick low-solidity layer in the middle.

The results for the second case are presented in Fig. 10. The two sample thicknesses were both tested with $n = 6$ equal thickness inner layers, i.e. $h_i = 2.7$ mm and $h_i = 4.3$ mm, $i = 1, \ldots, n$ for $h = 20$ mm and $h = 30$ mm, respectively. All other variables and the optimisation method remained the same.

The figure shows that a transitional layer with intermediate solidity appears next to the solid back layer in the solutions. The value of intermediate solidity depends on the mass available to the optimiser; for the thinner sample $s_1 = 0.701$, and for the thicker sample $s_1 = 0.282$. These optimised solutions can be seen as consisting of four layers: two solid layers on the outward faces, one thin transitional layer and one thick low-solidity layer in the middle, with most of the mass distributed at the back of the sample.

The maximum back face temperatures achieved for the optimised samples are summarised in Table 4. It can be seen that the optimal solutions with five variable thickness inner layers are more effective at reducing the back face temperature than those with six inner layers with equal
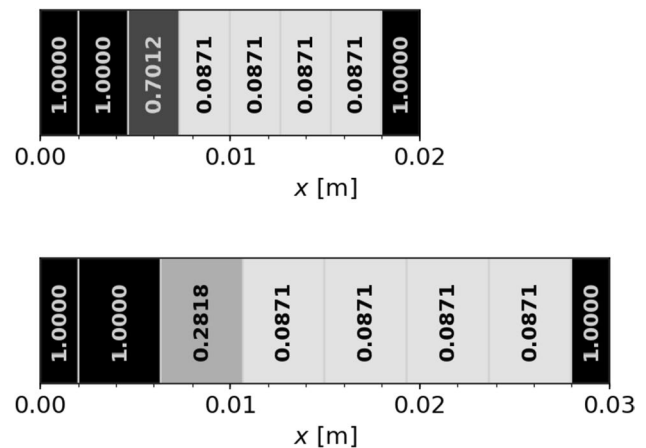
Fig. 10 The two optimised samples with six inner layers with equal thickness. The values for s are shown inside each layer—the denser the layer, the darker the shade

Table 4 Maximum back face temperature and associated Time instant for Optimised Designs

Thickness	Inner Layers	$\max(T_{\text{back}})$	$t(\max(T_{\text{back}}))$
20 mm	5, variable thickness	385.8 °C	469.25 s
	6, equal thickness	398.0 °C	451.10 s
30 mm	5, variable thickness	270.2 °C	769.43 s
	6, equal thickness	291.3 °C	845.60 s

thickness. Also, as expected for the 30 mm thick sample, reaching the maximum temperature on the back face takes more time. One limitation of this model is that thermal radiation within the lattice core was not considered. This would be a valid assumption for a lattice core filled with a lightweight material that blocks thermal radiation and has a negligible mass.

The open-cell structure was approximated by the analytical solidity relationships for a cubic cell structure. Future work could include revised functions that more closely match printed lattices. It is expected that this work could also be extended by optimisation of the lattice structure to maximise mechanical properties, for example mechanical strength (at elevated temperatures).

5 Conclusions

This work has revisited the published one-dimensional thermal analysis of a functionally graded titanium foam developed for thermal protection [18]. The previous model was adapted to solve for additively manufactured titanium alloy sandwich structures comprising an open-cell lattice core. This adapted model was experimentally validated for front face temperatures up to approximately 240 °C.

The adapted model was used to optimise the solidity profile of the lattice cores and to predict temperature profiles when applying transient heat fluxes of 100 kW m^{-2} for 180 s. It was shown that having a low-solidity/low-conductivity lattice closest to the face where heat flux is applied and a high solidity/high heat capacity at the back of the TPS is advantageous. In this way, the front face reaches the maximum temperature as fast as possible, and more heat is re-radiated. This result is in agreement with earlier findings [18].

The balance of heat capacity and effective conduction primarily governs the peak temperature at the back of the sandwich structure. The maximum back face temperature can be reduced by increasing the emissivity of the front face or increasing the heat capacity of the TPS. Increasing the heat capacity also delays the time at which the maximum back face temperature is reached.

Declarations

References

1. Ashby, M.: The properties of foams and lattices. Philos. Trans. Royal Soc. A Math. Phys. Eng. Sci. **364**(1838), 15–30 (2006). https://doi.org/10.1098/rsta.2005.1678

2. Balat-Pichelin, M., Annaloro, J., Barka, L., Sans, J.L.: Behavior of TiAl6V alloy at high temperature in air plasma conditions: Part 2-Thermal diffusivity and emissivity. J. Mater. Eng. Perform. **29**(7), 4606–4616 (2020). https://doi.org/10.1007/s11665-020-04985-6

3. Bapanapalli, S., Martinez, O., Gogu, C., Sankar, B., Haftka, R., Blosser, M.: Analysis and design of corrugated-core sandwich panels for thermal protection systems of space vehicles. In *47th AIAA/ASME/ASCE/AHS/ASC Structures, Structural Dynamics, and Materials Conference*, page 1942, (2006)

4. Basak, D., Overfelt, R.A., Wang, D.: Measurement of specific heat capacity and electrical resistivity of industrial alloys using pulse heating techniques. Int. J. Thermophys. **24**(6), 1721–1733 (2003)

5. Blosser, M.L.: Fundamental modeling and thermal performance issues for metallic thermal protection system concept. J. Spacecraft Rockets **41**(2), 195–206 (2004)

6. M. Boivineau, C. Cagran, D. Doytier, V. Eyraud, M.-H. Nadal, B. Wilthan, and P. G. Thermophysical properties of solid and liquid Ti-6Al-4V alloy. Int. J. Thermophys. 27 (2): 507–529, (2006). https://doi.org/10.1007/s10765-005-0001-6

7. Boyer, R.R.: An overview on the use of titanium in the aerospace industry. Mater. Sci. Eng. A **213**(1–2), 103–114 (1996)

8. Fang, X., Chen, J., Lu, B., Wang, Y., Guo, S., Feng, Z., Xu, M.: Optimized design of sandwich panels for integral thermal protection systems. Str. Multidiscip. Optim. **55**(1), 13–23 (2017)

9. Gogu, C., Bapanapalli, S.K., Haftka, R.T., Sankar, B.V.: Comparison of materials for an integrated thermal protection system for spacecraft reentry. J. Spacecraft Rockets **46**(3), 501–513 (2009)

10. Guo, Q., Wang, S., Hui, W., Li, Y., Xie, Z.: Thermo-mechanical optimization of metallic thermal protection system under aerodynamic heating. Structural and Multidisciplinary Optimization **61**(2), 819–836 (2020)

11. Incropera, F. P., DeWitt, D. P., Bergman, T. L., Lavine, A. S.: *Fundamentals of heat and mass transfer*, **6**. John Wiley (2007)

12. Lin, K., Hu, K., Gu, D.: Metallic integrated thermal protection structures inspired by the Norway spruce stem: Design, numerical simulation and selective laser melting fabrication. Optics Laser Technol. **115**, 9–19 (2019)

13. Mills, K.C.: Recommended values of thermophysical properties for selected commercial alloys. Woodhead Publishing Series in Metals and Surface Engineering, Cambridge, England 978-1-85573-569-9 (2002)

14. Pagan, A. S., Massuti-Ballester, B., Herdrich, G., Merrifield, J. A., Beck, J. C., Liedtke, V., Bonvoisin, B.: Investigation of the surface and boundary layer composition for demising aerospace materials. In: 7th Int. Workshop on Radiation of High Temperature Gases in Atmospheric Entry (2016)

15. Venkataraman, S., Blosser, M.: Optimal functionally graded metallic foam thermal insulation. AIAA J. **42**(11), 2355–2363 (2004)

16. Xu, Y., Xu, N., Zhang, W., Zhu, J.: A multi-layer integrated thermal protection system with C/SiC composite and Ti alloy lattice sandwich. Compos. Str. **230**, 111507 (2019)

17. Zhu, H., Sankar, B., Haftka, R., Venkataraman, S., Blosser, M.: Minimum mass design of insulation made of functionally graded material. J. Spacecraft Rockets **41**(3), 467–469 (2004). https://doi.org/10.2514/6.2002-1425

18. Zhu, H., Sankar, B., Haftka, R., Venkataraman, S., Blosser, M.: Optimization of functionally graded metallic foam insulation under transient heat transfer conditions. Str. Multidiscip. Optimiz. **28**(5), 349–355 (2004)